ACS APPLIED MATERIALS & INTERFACES

Research Article

www.acsami.org

Photoanode Current of Large–Area MoS_2 Ultrathin Nanosheets with Vertically Mesh–Shaped Structure on Indium Tin Oxide

Xiaoyong Xu,*[,†,‡] Jingguo Hu,*[,†] Zongyou Yin,[§] and Chunxiang Xu*[,‡]

[†]College of Physics Science and Technology, Yangzhou University, Yangzhou 225002, China

[‡]State Key Laboratory of Bioelectronics and School of Electronic Science and Engineering, Southeast University, Nanjing 210096, China

[§]School of Materials Science and Engineering, Nanyang Technological University, 50 Nanyang Avenue, Singapore 639798, Singapore

Supporting Information

ABSTRACT: A large area of hydrothermally grown MoS_2 ultrathin nanosheets (NSs) with a vertically mesh-shaped structure on indium tin oxide (ITO) substrate was directly used as the photoanode of a potoelectrochemical (PEC) cell. The photoelectrocatalytic capacity of ultrathin MoS_2 NSs was demonstrated, which was attributed not only to the excellent electrocatalytic activity originating from the exposed preferentially active edge sites but also to the superior photoelectric response resulting from the large light absorption of ultrathin MoS_2 NSs and from the efficient separation of electron–hole pairs at the ITO/MoS_2 interfaces. The significantly enhanced photocurrent indicates that the MoS_2 ultrathin NSs can be a promising photoelectrocatalyst for PEC cells, unveiling the potential of MoS_2-based PEC cells for solar energy absorption and conversion.

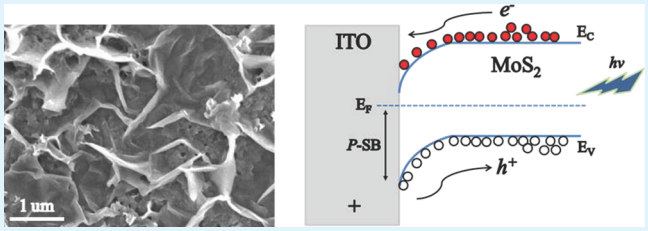

KEYWORDS: *MoS_2, potoelectrochemical cells, photoelectrocatalysis, hydrothermal method, two-dimensional nanosheets, photo-generated carrier dynamics*

INTRODUCTION

Photoelectrochemical (PEC) solar cells, which produce photovoltaic effect or water splitting at the semiconductor–electrolyte interface, have received enormous research interests because of the potential of solar energy conversion with two outstanding natures of carbon-free emissions and renewable sources.[1−4] The single- and multi-junction PEC cells of semiconductors, such as TiO_2, ZnO, Si, CuO, etc., have been elaborately designed to harvest more sunlight and to improve carrier separation.[4−8] However, the interfaces between most semiconductors and electrolyte have poor electrocatalytic active because of kinetic limitations,[3] indicating that a good photocatalyst is not necessarily a good PEC catalyst.[9] Thus, a most active Pt electrocatalyst is normally modified on the surface of PEC cells to achieve the combination of the electro- and photocatalyses, and it is shown that such a functional integration is important to enhance the efficiency and stability of PEC cells.[10,11] The recently reported results have confirmed the electrocatalytic activity of MoS_2 NSs in the hydrogen evolution reaction (HER), which makes MoS_2 a promising alternative for expensive Pt electrocatalyst.[12−16] Meanwhile, many theoretical and experimental investigations have found transition metal dichalcogenides (TMDs) have some unique optical properties. For example, the layer-modulated band gap can capture more solar photons with different energies;[17,18] the nesting band induces a strong interband absorption above the fundamental band gap;[19,20] the heavy effective mass of d electrons and van Hove singularity in the electronic density of states enhance photon–electron interaction.[21,22] We note that there is no one of these natures being not conducive for the sunlight absorption and the photoelectric conversion, as Eda[20] and Grossman[22] recently reported few-layered MoS_2-based optoelectronics. More recently, the photocatalytic activity of MoS_2 ultrathin NSs has been demonstrated;[23,24] however, as far as we know, the few-layered MoS_2-based PEC cells have been rarely reported so far.

In this work, a whole scale of ultrathin MoS_2 NSs with a vertically mesh-shaped structure fabricated directly on indium tin oxide (ITO) substrate by a hydrothermal method, as a proof-of-concept application, was employed as a tandem photoanode of the PEC cell to examine the photogenerated carrier dynamics in the PEC catalysis. MoS_2 ultrathin NSs with an integration of electro- and photocatalyses were demonstrated as a superior photoelectrocatalyst for PEC cells, illustrating new avenues for solar energy conversion by implanting ultrathin MoS_2 NSs into PEC cells.

EXPERIMENTAL SECTION

The hydrothermal synthesis of MoS_2 nanosheets on indium tin oxide (ITO) was described as following. Typically, sodium molybdate (0.06 mmol, $Na_2MoO_4{\cdot}2H_2O$) and thioacetamide (0.4 mmol, C_2H_5NS)

Received: February 25, 2014
Accepted: March 31, 2014
Published: March 31, 2014

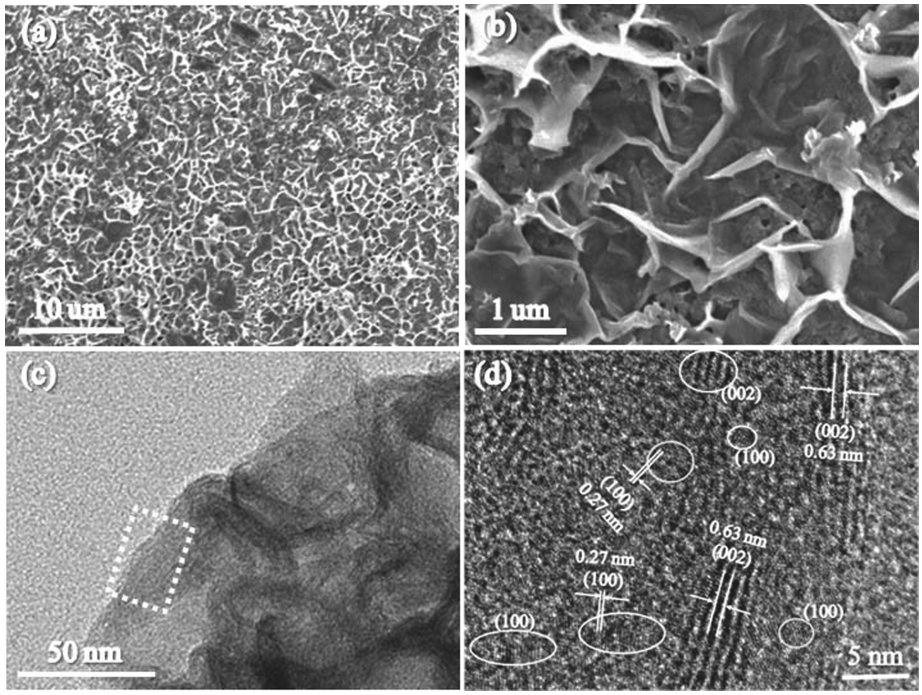

Figure 1. (a) Low-magnification and (b) high-magnification FESEM (c) TEM images of MoS_2 NSs. (d) HRTEM image of the region denoted by white line in c, showing two lattice spacings of 0.63 and 0.27 nm corresponding to interlayer (002) and interplanar (100) planes of hexagonal MoS_2, respectively.

were dissolved in deionized water (20 mL) under vigorous ultrasound to form a homogeneous solution. The solution was then transferred into a Teflon-lined stainless steel autoclave (25 mL), and a piece of cleaned ITO substrate (1 cm × 2 cm) was immersed into the solution and was placed face down with a tilted angle against the wall. Subsequently, the autoclave was put into an electric oven and was heated at 220 °C for 20 h. The grown product on ITO was washed with deionized water and absolute ethanol several times to remove any possible ions, and then dried at room temperature under vacuum.

Field-emission scanning electron microscopy (FESEM) was performed using a JEOL JSM-7600F equipped with energy dispersive X−ray spectroscopy (EDS) under an accelerating voltage of 5 kV. Transmission electron microscopy (TEM) and high-resolution TEM (HRTEM) were carried out on a JEOL JEM 2010F with the beam energy of 200 keV. UV−vis absorption spectrum was conducted on a UV-2501 spectrophotometer. X−ray diffraction (XRD) patterns were recorded by using a Siemens D-500 X−ray diffractometer with Cu Kα (λ = 0.15406 nm). X-ray photoelectron spectroscopy (XPS) was performed using an X-ray photoelectron Spectrometer (KRATOS, AXIS ULTRA) with a monochromated Al Kα (1486.7 eV) X-ray source at a power of 150 W (15 kV × 10 mA). The binding energy of C 1s peak at 285.0 eV was used as the reference for all the spectra.

Using an electrochemical workstation (CHI852c, CH Instruments), photocurrent measurements were performed in a photoelectrochemical (PEC) cell with a three-electrode configuration, consisting of our synthesized sample as working electrode (WE), Ag/AgCl as reference electrode (RE) and Pt-wire as counter electrode (CE), respectively. A 100 W halogen−lamp light source (Dolan Jenner, Model 150 Illuminator) with a cutoff filter of 420 nm was used to simulate the solar illumination. As the buffer solution we used 0.1 M KH_2PO_4 solution in Milli-Q water (18 M Ω cm) with pH adjusted to 7.0.

RESULTS AND DISCUSSION

The as−synthesized MoS_2 NSs cover the entire ITO substrate. The FESEM image in Figure 1a shows that large-scale NSs with network structure uniformly grows on the substrate. Moreover, the amplified FESEM image shown in Figure 1b reveals that the as-grown NSs have ultrathin morphology, and they do not assemble each other. More importantly, these NSs present an almost vertical alignment, forming the vertically mesh-shaped structure with preferentially exposed edges. Noting that the edge of MoS_2 has been identified as the active site for electrocatalyses,[25] furthermore Jaramillo[26] and Cui et al.[27] have reported recently the significantly enhanced HER performance by engineering MoS_2 arrangement to preferentially expose active edge sites, respectively. Thus, the abundant active edge sites exposed in present NSs network must endow MoS_2 the higher electrocatalytic activity. In addition, such a three-dimensional (3D) mesh structure exposes meanwhile the large surface area, which is significantly conducive to the optical absorption and the redox reaction. The typical TEM image, as shown in Figure 1c, also verifies the lamellar NSs morphology. Figure 1d shows the corresponding HRTEM image in the region denoted by the white line in Figure 1c. The observed lattice spacings of 0.63 and 0.27 nm correspond to the interlayer (002) and interplanar (100) planes of hexagonal MoS_2, respectively. Particularly, the crystal fringes of (002) plane along the curled edge indicate the formation of 3−5 layered MoS_2 ultrathin NSs. The EDS spectrum shown in Figure S1a in the Supporting Information illustrates that the grown NSs are composed of characteristic Mo and S elements, and some other detected elements including Si, In, Ca, and O are originated from the ITO substrate. The XPS survey spectrum in Figure S1b in the Supporting Information is also dominated by the stoichiometric Mo and S peaks besides some peaks of inevitable C and O elements. To confirm further phase structure and chemical state, the XRD and high-resolution XPS measurements were performed. Figure 2a shows the XRD pattern of sample, in which the standard pattern of hexagonal MoS_2 phase (JCPDS card No. 73−1508) and the XRD pattern of bare ITO substrate are imported as references. In addition to some strong diffraction peaks coming from ITO, there are other peaks corresponding respectively to (002), (004), (100),

dx.doi.org/10.1021/am501159s | ACS Appl. Mater. Interfaces 2014, 6, 5983−5987

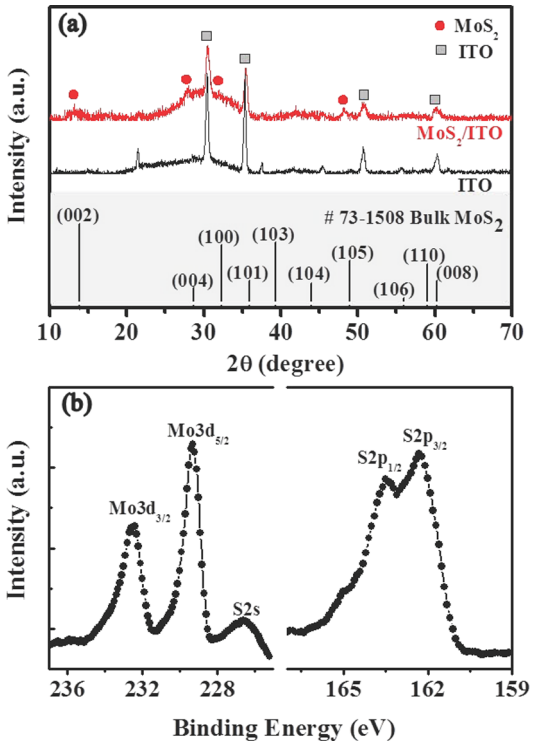

Figure 2. (a) XRD patterns of the MoS_2/ITO and bare ITO with the standard pattern of hexagonal MoS_2 as a reference. (b) High-resolution XPS spectra in Mo 3d, S 2s, and S 2p regions of MoS_2 NSs.

and (105) planes of standard hexagonal phase MoS_2, confirming the formation of MoS_2 crystalline phase. It is reasonable that the diffraction peaks of MoS_2 are weaker and broader than that of ITO because the ultrathin MoS_2 NSs usually cannot be detected intensively by XRD.[28] Especially, the extremely weak (002) peak of *c*-plane can support in turn that the produced MoS_2 NSs are of ultrathin structure.[28] The high-resolution XPS spectra in Mo 3d and S 2p regions, as shown in Figure 2b, identify respectively the Mo $3d_{3/2}$ peak of 232.4 eV, Mo $3d_{5/2}$ peak of 229.3 eV, S $2p_{1/2}$ of 163.5 eV, and S 2p3/2 peak of 162.3 eV, indicating further the chemical composition of MoS_2 in the sample.

Figure 3a shows the UV−vis absorption spectrum of the as-synthesized MoS_2 NSs. Two obvious absorption peaks respectively locate at the UV and visible bands, moreover, the intensity of absorbing UV is much higher than that of absorbing visible light despite the small band gap (1.2−1.8 eV)[29,30] of MoS_2 NSs. Indeed, many experiments also found that there is

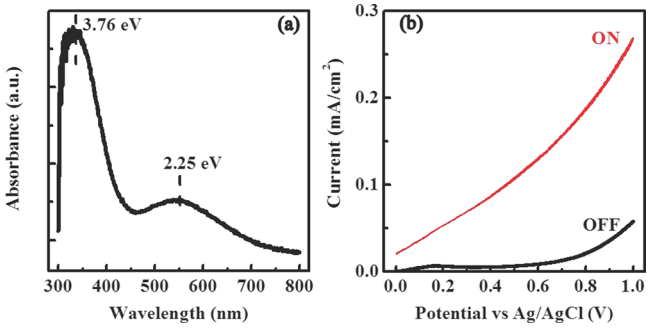

Figure 3. (a) UV−vis absorption spectrum and (b) linear sweep voltammograms in the dark and under illumination for MoS_2 NSs.

such a multipeak-absorption feature in few-layered MoS_2 NSs; furthermore, the strong absorption peaks are usually above the fundamental band gap.[31] Recently, the theoretical calculations of Carvalho[19] and Grossman et al.[22] suggested that the large optical absorption above the fundamental band gap is a general character in two-dimensional (2D) TMDs, which was explained by both the strong dipole transition between localized d orbits and the band nesting enhanced by van Hove singularities in the electronic density of states. These natures undoubtedly enable 2D TMD like MoS_2 strong photon−electron coupling, leading to large photoelectric response. In addition, MoS_2 undergoes a crossover from indirect to direct gap when going from multilayer to monolayer, inducing enhanced photoluminescence (PL) via recombination at the direct gap of monolayer.[29,30] For photovoltaics (PV) and photocatalysis, such a direct recombination of photo−generated carriers is highly undesirable. Thus, the present few-layered MoS_2 NSs can not only guarantee the light absorption and the exposed active edge but also restraint the direct recombination of electron−hole pairs. On the basis of these analyses, the few-layered MoS_2 NSs are possibly entailed novel and comprehensive capacities of absorbing and converting the broadband sunlight for PV and PEC devices. As a proof-of-concept application, we use the ultrathin MoS_2 NSs as the photoanode of PEC cell to examine the photocurrent characteristics. Figure 3b shows the linear sweep voltammograms, where the black and red lines represent the current density in the dark and under illumination, respectively. The largely enhanced photocurrent can be seen at any external potentials, indicating the effective incorporation of photocatalytic activity. Figure S2 in the Supporting Information adds the linear voltammograms of bare ITO substrate in the dark and under illumination, and almost no photocurrent response is detected, excluding the contribution from ITO. Noting that the accelerated rising of dark current curve after an onset potential of about 0.6 V represents the sample's electrocatalytic effect. For the other special case, when without the external potential, the current increases by about 50 times only because of the illumination, which denotes the pure photocatalytic activity. However, although only the MoS_2 NSs are the photo-response active material, the interface between ITO and MoS_2 also plays an important role in separating photo−generated carriers for PEC catalyses. Figure 4 shows the energy band alignment at the ITO/MoS_2 interface. Because ITO is a (semi)metal and MoS_2 is a semiconductor, the electrons and holes generated in such a PEC cell would be separated through the Schottky barrier (SB) formed at the ITO/MoS_2 interface. According to the previous

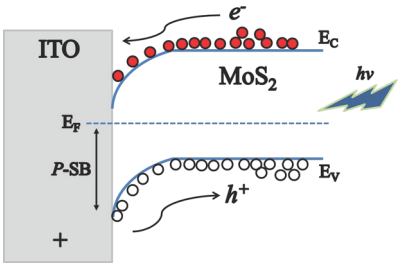

Figure 4. Schematic energy band diagram of the MoS_2/ITO interface. *p*-SB is the hole Schottky barrier, and E_C and E_V are the conduction and valence band edges, respectively. The electrons and holes with their reverse transporting directions under illumination are respectively denoted by solid and hollow circles.

dx.doi.org/10.1021/am501159s | ACS Appl. Mater. Interfaces 2014, 6, 5983−5987

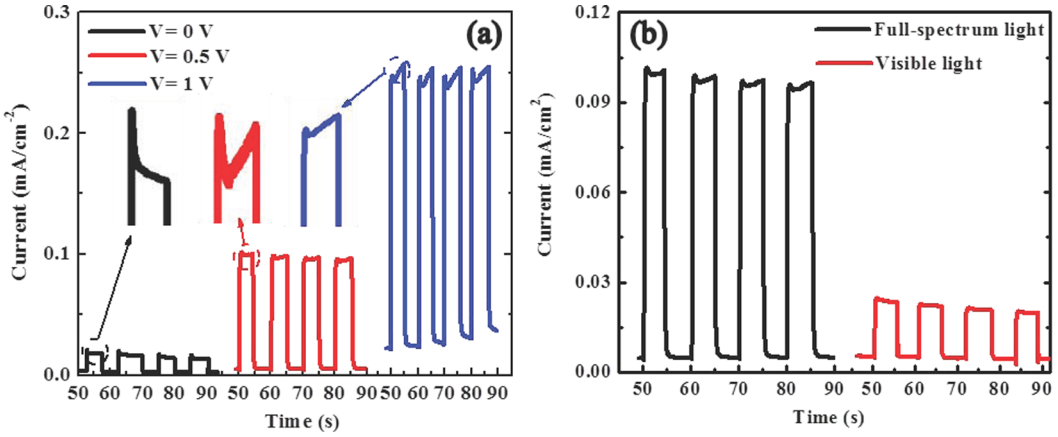

Figure 5. Amperometric $I-t$ curves (a) at several typical potentials of 0, 0.5, and 1 V, and (b) under full-spectrum and visible lights at a potential of 0.5 V.

reports,[15,22] the band gap of $E_g \approx 1.8$ eV and a workfunction of $\phi_{MoS_2} \approx 5.2$ eV for few-layered MoS_2 NSs were assumed, and the workfunction of $\phi_{ITO} \approx 4.4$ eV for ITO was set. The carrier separation occurs by injecting photogenerated electrons from the conduction band of MoS_2 to ITO, whereas holes photogenerated in the valence band of MoS_2 cannot diffuse to ITO because of the existence of p-type SB. The reverse transporting of positive and negative charge carriers at the MoS_2/ITO interface retards the recombination of electron−hole pairs and prolongs the carrier lifetime, leading to the superior photocurrent response.

Figure 5a shows the transient current under the chopped light illumination at several typical potentials of 0, 0.5, and 1 V. The currents always exhibit good switching behaviors with the pulsed illumination at any one potential, indicating further the photocurrent can be reproducibly enhanced by increasing potential or by introducing light illumination. More importantly, it can be seen that the effects of potential and light illumination can promotes each other, and a superior photocurrent of 0.26 mA/cm^{-2} can be achieved at 1 V potential. The overshooting behavior of photocurrent amplified in the inset of Figure 5a reveals further the synergistic effect between the external potential and light illumination. The current overshoots only when switching on light, indicating an instantaneous accumulation of photo-separated electrons/holes on the NSs surface, and if no one proper potential drives them to flow towards opposite directions, the part of them will subsequently lost via the nonradiative transition and the radiative recombine, then the photocurrent decays rapidly until a stationary photocurrent is reached. Thus, the remarkable overshooting feature in the absence of external potential reflects the large concentration of photo−generated carriers, and it can gradually calm down with the potential increasing, demonstrating fully the potential−assisted charge separation. These are very important for improving the photocurrent and consequently the PEC performace. To identify the effective light band for the photoelectrocatalysis of our MoS_2 NSs, Figure 5b compares the transient photocurrents under the full-spectrum light from a halogen lamp and the visible light with wavelengths longer than 420 nm selected by a filter. This result suggests that about 76% photocurrent arises from UV band although the visible light is also contributing, which is consistent with the above optical absorption feature. Therefore, it will motivate one to design further MoS_2-based heterojunction PEC cells for solar energy conversion by integrating the complementary materials as visible light absorbers.

CONCLUSIONS

In summary, we synthesized a large area of MoS_2 ultrathin nanosheets (NSs) with a vertically mesh-shaped structure on ITO substrates as the photoanode of a PEC cell. The dynamic process of photogenerated carriers was illustrated, which involves the photon absorption and conversion in ultrathin MoS_2 NSs, and the charge separation driven by the matched energy band and the external potential at MoS_2/ITO interfaces. The significantly enhanced photocurrent demonstrates the photoelectrocatalytic activity of untrathin MoS_2 NSs, highlighting the promising potential of the MoS_2 NSs-based PEC cells for photoelectrocatalytic energy conversion and degradation.

ASSOCIATED CONTENT

Supporting Information

EDX spectrum, XPS survey spectrum of MoS_2 NSs grown on ITO, and linear voltammograms of MoS_2/ITO and bare ITO substrate in the dark and under illumination. This material is available free of charge via the Internet at http://pubs.acs.org.

AUTHOR INFORMATION

Corresponding Authors

*E-mail: xxy@yzu.edu.cn.
*E-mail: jghu@yzu.edu.cn.
*E-mail: xcxseu@seu.edu.cn.

Author Contributions

The manuscript was written through contributions of all authors. All authors have given approval to the final version of the manuscript.

Notes

The authors declare no competing financial interest.

ACKNOWLEDGMENTS

This work was supported by National Natural Science Foundation of China (11104240 and 60725413), "973" Program (2011CB302004 and 2013CB932903), and Jiangsu Government Scholarship for Overseas Studies in 2013.

REFERENCES

(1) Gray, H. B. Powering The Planet with Solar Fuel. *Nat. Chem.* **2009**, *1*, 7.

(2) Kargar, A.; Sun, K.; Jing, Y.; Choi, C.; Jeong, H.; Zhou, Y.; Madsen, K.; Naughton, P.; Jin, S.; Jung, G. Y.; Wang, D. Tailoring n-ZnO/p-Si Branched Nanowire Heterostructures for Selective Photoelectrochemical Water Oxidation or Reduction. *Nano Lett.* **2013**, *13*, 3017−3022.

(3) Walter, M. G.; Warren, E. L.; McKone, J. R.; Boettcher, S. W.; Mi, Q.; Santori, E. A.; Lewis, N. S. Solar Water Splitting Cells. *Chem. Rev.* **2010**, *110*, 6446−6473.

(4) Yin, Z. Y.; Wang, Z.; Du, Y. P.; Qi, X. Y.; Huang, Y. Z.; Xue, C.; Zhang, H. Full Solution-Processed Synthesis of All Metal Oxide-Based Tree-like Heterostructures on Fluorine-Doped Tin Oxide for Water Splitting. *Adv. Mater.* **2012**, *24*, 5374−5378.

(5) Kargar, A.; Sun, K.; Jing, Y.; Choi, C.; Jeong, H.; Jung, G. Y.; Jin, S.; Wang, D. 3D Branched Nanowire Photoelectrochemical Electrodes for Efficient Solar Water Splitting. *ACS Nano* **2013**, *7*, 9407−9415.

(6) Wang, D.; Pierre, A.; Kibria, M. G.; Cui, K.; Han, X.; Bevan, K. H.; Guo, H.; Paradis, S.; Hakima, A. R.; Mi, Z. Wafer-Level Photocatalytic Water Splitting on GaN Nanowire Arrays Grown by Molecular Beam Epitaxy. *Nano Lett.* **2011**, *11*, 2353−2357.

(7) Kibria, M. G.; Nguyen, H. P. T.; Cui, K.; Zhao, S.; Liu, D. P.; Guo, H.; Trudeau, M. L.; Paradis, S.; Hakima, A. R.; Mi, Z. One-Step Overall Water Splitting under Visible Light Using Multiband InGaN/GaN Nanowire Heterostructures. *ACS Nano* **2013**, *7*, 7886−7893.

(8) Warren, S. C.; Voïtchovsky, K.; Dotan, H.; Leroy, C. M.; Cornuz1, M.; Stellacci, F.; Hébert, C.; Rothschild, A.; Grätzel, M. Identifying Champion Nanostructures for Solar Water-Splitting. *Nat. Mater.* **2013**, *12*, 842−849.

(9) Hou, Y. D.; Abrams, B. L.; Vesborg, P. C. K.; Bjorketun, M. E.; Herbst, K.; Bech, L.; Setti, A. M.; Damsgaard, C. D.; Pedersen, T.; Hansen, O.; Rossmeisl, J.; Dahl, S.; Norskov, J. K.; Chorkendorff, I. Bioinspired Molecular Co-catalysts Bonded to A Silicon Photocathode for Solar Hydrogen Evolution. *Nat. Mater.* **2011**, *10*, 434−438.

(10) Boettcher, S. W.; Warren, E. L.; Putnam, M. C.; Santori, E. A.; Turner-Evans, D.; Kelzenberg, M. D.; Walter, M. G.; McKone, J. R.; Brunschwig, B. S.; Atwater, H. A.; Lewis, N. S. Photoelectrochemical Hydrogen Evolution Using Si Microwire Arrays. *J. Am. Chem. Soc.* **2011**, *133*, 1216−1219.

(11) Heller, A.; Aharon-Shalom, E.; Bonner, W. A.; Miller, B. Hydrogen-Evolving Semiconductor Photocathodes: Nature of The Junction and Function of The Platinum Group Metal Catalyst. *J. Am. Chem. Soc.* **1982**, *104*, 6942−6948.

(12) Xie, J. F.; Zhang, H.; Li, S.; Wang, R. X.; Sun, X.; Zhou, M.; Zhou, J. F.; Lou, X. W.; Xie, Y. Defect-Rich MoS_2 Ultrathin Nanosheets with Additional Active Edge Sites for Enhanced Electrocatalytic Hydrogen Evolution. *Adv. Mater.* **2013**, *25*, 5807−5813.

(13) Chhowalla1, M.; Shin, H. S.; Eda, G.; Li, L. J.; Loh, K. P.; Zhang, H. The Chemistry of Two-Dimensional Layered Transition Metal Dichalcogenide Nanosheets. *Nat. Chem.* **2013**, *5*, 263−275.

(14) Lukowski, M. A.; Daniel, A. S.; Meng, F.; Forticaux, A.; Li, L.; Jin, S. Enhanced Hydrogen Evolution Catalysis from Chemically Exfoliated Metallic MoS_2 Nanosheets. *J. Am. Chem. Soc.* **2013**, *135*, 10274−10277.

(15) Song, X. F.; Hu, J. L.; Zeng, H. B. Two-Dimensional Semiconductors: Recent Progress and Future Perspectives. *J. Mater. Chem. C* **2013**, *1*, 2952−2969.

(16) Huang, X.; Zeng, Z. Y.; Bao, S. Y.; Wang, M. F.; Qi, X. Y.; Fan, Z. X.; Zhang, H. Solution-Phase Epitaxial Growth of Noble Metal Nanostructures on Dispersible Single-Layer Molybdenum Disulfide Nanosheets. *Nat. Commun.* **2013**, *4*, 1444.

(17) Polman, A.; Atwater, H. A. Photonic Design Principles for Ultrahigh-Efficiency Photovoltaics Nature Materials. *Nat. Mater.* **2012**, *11*, 174−177.

(18) Lee, H. S.; Min, S. W.; Chang, Y. G.; Park, M. K.; Nam, T.; Kim, H.; Kim, J. H.; Ryu, S.; Im, S. MoS_2 Nanosheet Phototransistors with Thickness-Modulated Optical Energy Gap. *Nano Lett.* **2012**, *12*, 3695−3700.

(19) Carvalho, A.; Ribeiro, R. M.; Neto, A. H. C. Band Nesting and The Optical Response of Two-Dimensional Semiconducting Transition Metal Dichalcogenides. *Phys. Rev. B* **2013**, *88*, 115205.

(20) Eda, G.; Maier, S. A. Two-Dimensional Crystals: Managing Light for Optoelectronics. *ACS Nano* **2013**, *7*, 5660−5665.

(21) Britnell, L.; Ribeiro, R. M.; Eckmann, A.; Jalil, R.; Belle, B. D.; Mishchenko, A.; Kim, Y.-J.; Gorbachev, R. V.; Georgiou, T.; Morozov, S. V.; Grigorenko, A. N.; Geim, A. K.; Casiraghi, C.; Castro Neto, A. H.; Novoselov, K. S. Strong Light-Matter Interactions in Heterostructures of Atomically Thin Films. *Science* **2013**, *340*, 1311−1314.

(22) Bernardi, M.; Palummo, M.; Grossman, J. C. Extraordinary Sunlight Absorption and One Nanometer Thick Photovoltaics Using Two-Dimensional Monolayer Materials. *Nano Lett.* **2013**, *13*, 3664−3670.

(23) Quinn, M. D. J.; Ho, N. H.; Notley, S. M. Aqueous Dispersions of Exfoliated Molybdenum Disulfide for Use in Visible-Light Photocatalysis. *ACS Appl. Mater. Interfaces* **2013**, *5*, 12751−12756.

(24) Maitra, U.; Gupta, U.; De, M.; Datta, R.; Govindaraj, A.; Rao, C. N. R. Highly Effective Visible-Light-Induced H_2 Generation by Single-Layer 1T-MoS_2 and a Nanocomposite of Few-Layer 2H-MoS_2 with Heavily Nitrogenated Graphene. *Angew. Chem., Int. Ed.* **2013**, *52*, 1−6.

(25) Jaramillo, T. F.; Jørgensen, K. P.; Bonde, J.; Nielsen, J. H.; Horch, S.; Chorkendorff, I. Identification of Active Edge Sites for Electrochemical H_2 Evolution from MoS_2 Nanocatalysts. *Science* **2007**, *317*, 100−102.

(26) Kibsgaard, J.; Chen, Z.; Reinecke, B. N.; Jaramillo, T. F. Engineering The Surface Structure of MoS_2 to Preferentially Expose Active Edge Sites for Electrocatalysis. *Nat. Mater.* **2012**, *11*, 963−969.

(27) Kong, D.; Wang, H.; Cha, J. J.; Pasta, M.; Koski, K. J.; Yao, J.; Cui, Y. Synthesis of MoS_2 and $MoSe_2$ Films with Vertically Aligned Layers. *Nano Lett.* **2013**, *13*, 1341−1347.

(28) Zeng, Z. Y.; Yin, Z. Y.; Huang, X.; Li, H.; He, Q. Y.; Lu, G.; Boey, F.; Zhang, H. Single-Layer Semiconducting Nanosheets: High-Yield Preparation and Device Fabrication. *Angew. Chem. Int. Ed.* **2011**, *50*, 11093−11097.

(29) Splendiani, A.; Sun, L.; Zhang, Y. B.; Li, T. S.; Kim, J.; Chim, C. Y.; Galli, G.; Wang, F. Emerging Photoluminescence in Monolayer MoS_2. *Nano Lett.* **2010**, *10*, 1271−1275.

(30) Mak, K. F.; Lee, C.; Hone, J.; Shan, J.; Heinz, T. F. Atomically Thin MoS_2: A New Direct-Gap Semiconductor. *Phys. Rev. Lett.* **2010**, *105*, 136805.

(31) Eda, G.; Yamaguchi, H.; Voiry, D.; Fujita, T.; Chen, M.; Chhowalla, M. Photoluminescence from Chemically Exfoliated MoS_2. *Nano Lett.* **2011**, *11*, 5111−5116.